Analyzing the Influence of Microstructure on the Mechanical Properties of TIG Welded Joints processed by Friction Stir considering the sampling Orientation

Velaphi Msomi
Department of Mechanical Engineering, College of Science, Technology, and Engineering, Florida Campus, University of South Africa, South Africa
msomiv@gmail.com (corresponding author)

Sipokazi Mabuwa
Mechanical and Mechatronic Engineering Department, Faculty of Engineering and the Built Environment, Cape Peninsula University of Technology, South Africa
sipokazimabuwa@gmail.com

Received: 30 September 2023 | Revised: 15 October 2023 | Accepted: 16 October 2023

 DOI: https://doi.org/10.48084/etasr.6459

ABSTRACT

The contribution of the microstructural arrangement to the mechanical properties of friction stir processed Tungsten Inert Gas (TIG) welded joints is reported in this work. The TIG-welded joints were subjected to a single pass of Friction Stir Processing (FSP). The friction stir processed joint was sampled transversally and longitudinally, and different tests were conducted and studied comparatively. The microstructural analysis showed refined grains with varying degrees. The mean grain size for the transversally sampled specimen was found to be 11.48 µm, while the longitudinally sampled specimen had varying mean grain size from 7.32 µm to 15.09 µm. The varying mean grain size of the longitudinally sampled specimen is caused by the staggered arrangement of the microstructure. The tensile properties and the microhardness of the transversally sampled specimen were lower than those of the longitudinally sampled specimen. The ultimate tensile strength of the transversally sampled specimen was found to be 87.88 MPa which is lower than that of the longitudinally sampled specimen (133.83 MPa). The microhardness of the longitudinally sampled specimen fluctuated between 30 HV and 80 HV while the transversally sampled specimen had a maximum microhardness of approximately 57 HV.

Keywords-friction stir processing; sampling directions; microstructure; tensile strength; tungsten inert gas welding

I. INTRODUCTION

Tungsten Inert Gas (TIG) welding is a well-known joining technique best suited for soft metals like aluminum, copper, and magnesium [1, 2]. This technique operates on the principle of melting another metal with similar properties to the joined materials. The fact that there is high heat input involved in the procedure suggests that there are opportunities for the post-defects that can compromise the quality of the formed joint [3, 4]. This suggests that there is a need for the post-treatment required when one wants to enhance the quality of the produced or existing joint. There are many post-treatments that one can employ in enhancing the joint. This includes high-temperature and solid-state-based treatments like friction stir processing [5-7]. Friction Stir Processing (FSP) is a solid state-based microstructural modifying technique that uses friction to generate the heat required to soften the material for microstructural modification [8]. FSP is a Friction Stir Welding (FSW) variant, but the distinction is that FSP requires or operates on a single surface, while FSW operates on more than one surface [9-12]. The FSP technique has been employed to modify the surface of metals by enforcing foreign particles and forming surface composites [13-16]. However, recent developments have shown that this technique can be employed in processing the joints produced using different techniques.

Authors in [17] have reported the influence of subjecting AA5083-H111 T-joints produced through gas metal arc welding to friction stir processing procedure. It should be noted that the FSP procedure was employed at the toe of the GMAW welds. The microstructural analysis revealed a clear grain variation from the weld to the processed area. The refinement of grains in the processed area resulted in improved hardness

and tensile properties compared to the weld. There was also a notable increase in fatigue life for the processed weld compared to the unprocessed weld. The unprocessed weld showed multi-nucleation site post fatigue test, whereas the processed joint showed significantly lower nucleation sites. The impact of applying FSP on the TIG welded joints was investigated in [18]. The normal procedure was used to produce TIG welded joints and later subjected to the FSP procedure. The microstructural analysis showed significant grain refinement at the nugget zone post-FSP procedure. This grain refinement contributed immensely towards enhancing tensile and microhardness properties compared to the TIG welded joint. However, it was observed that the mechanical properties of the base metal remained higher compared to friction stir processed TIG-welded joint and unprocessed TIG-welded joint. Authors in [19] analyzed the FSP procedure's influence on the AA6061/AA7075 TIG welded joints. The analysis conducted in this study included the prediction of heat transfer with the use of ANSYS software. The analysis also involved the variation of FSP parameters. It was discovered that the increase in rotational speed contributed to the refinement of grains and also impacted the heat input. This resulted in a reduction of residual stress while maximizing the tensile strength and hardness of the joint. It should be noted that all the samples tested in this study were sampled perpendicular to the welding direction.

The influence of FSP on the friction stir welded joints was investigated in [20]. The friction stir welded plates were subjected to the FSP procedure using the same welding setup. The microstructural analysis showed moderate grain refinement compared to the friction stir welded joint. A slight increase in mechanical properties was observed on the processed joints in comparison with the unprocessed ones. However, the mechanical properties of the joints were all less than those of the AA6082 base metal. All the analyses were performed on specimens sampled perpendicular to the welding direction. There are a few more studies where the FSP was employed on the joints [21-25]. However, it has been observed that most tests associated with joint analysis are performed on samples sampled perpendicular to the welding direction. This kind of analysis does not give full information about the actual joint. The information obtained in these analyses is mixed with the information outside the joint.

The current paper investigates the mechanical properties of the TIG welded joint when subjected to the FSP process. The main focus is on the analysis of the joint's behavior, considering the sampling direction, i.e. longitudinal and transversal. This kind of analysis could be useful to understand the strength of the joint and better configure components made from materials considered in this work.

II. MATERIALS AND METHODS

AA8011 and AA6082 plates were utilized, each 6 mm thick. These plates were initially prepared into rectangular shapes of 250 mm × 50 mm, with their end edges shaped into a V configuration of 60^o in preparation for TIG welding. The welding process employed ER4043 filler material, the chemical composition of which was measured using Belec Spectroscopy [25] and is detailed in Table I. During welding, argon gas was maintained at a flow rate of 28 L/min, the welding speed was set at 42 mm/min, and voltage and current were controlled at 37 V and 152 A, respectively. The FSP was conducted using the semi-automated LAGUN FA.1-LA milling machine [26]. FSP was executed with a tool rotational speed of 1100 rpm, a traverse speed of 55 mm/min, and a tilt angle of 2^o. The tool used for the FSP procedure was produced from high-speed steel with a triangular-fluted pin profile, which was 5.8 mm long and with a diameter of 7 mm, as illustrated in Figure 1. Figure 2 illustrates a schematic diagram of the friction stir processed TIG-welded plate, with AA6082 positioned on the retreating side and AA8011 on the advancing side.

TABLE I. CHEMICAL COMPOSITION OF THE WIRE FILLER [25]

Metal	Si	Fe	Cu	Mn	Mg	Cr	Ti	Zn	Al
ER4043	5.2	0.75	0.31	0.04	0.04	0.01	0.15	0.1	Bal

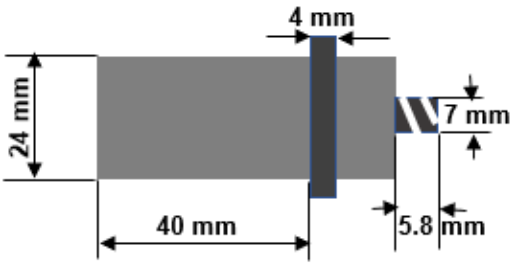

Fig. 1. Schematic diagram of the FSP tool.

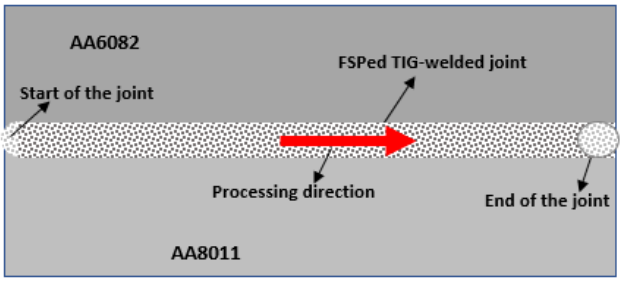

Fig. 2. Schematic diagram of the friction stir processed TIG-welded plate.

Waterjet technology was employed to prepare specimens for various tests, each test requiring both transverse and longitudinal sampling, as depicted in the schematic representation in Figure 3. Tensile testing was carried out using the Hounsfield 25K tensile machine, which was equipped with Horizon software. This specialized software is designed to directly extract tensile properties from the machine, eliminating the need for data postprocessing. The design and execution of the tensile tests adhered to the ASTM E8M-04 standard. Post tensile testing, the fractured surfaces were subject to analysis using scanning electron microscopy. Microhardness testing was performed using the InnovaTest Falcon 500 hardness testing machine, following the guidelines outlined in the ASTM E384-11 standard. All samples were subjected to a 300 g load with a dwell time of 10 s. To delve into the microstructural arrangement, the Motic AE2000 optical metallurgical microscopy was utilized, and grain visualization was achieved by applying two different etchants: a modified Keller's agent

for AA8011 which was found to be more effective and Weck's agent for AA6082. This combination ensured a clear and uniform grain structure throughout the entire stir zone without any over-etched regions [24]. Grain size measurements were conducted using ImageJ software, employing the linear intercept method, and subsequent calculations were carried out based on the acquired data. This grain measurement approach was adapted from the ASTME112-12 standard [25].

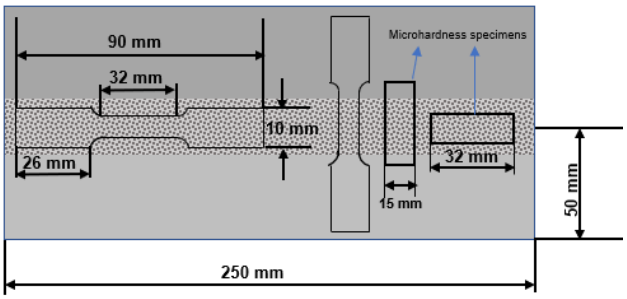

Fig. 3. Schematic diagram depicting the sampling directions of different test samples.

III. RESULTS AND DISCUSSION

This section deals with the comparative analysis and discussion of the obtained results from the longitudinal and transverse directions.

A. Microstructure

Figure 4 illustrates the microstructural arrangement within the stir zone of the friction stir-processed TIG-welded joint. Specifically, Figure 4(a) provides a view of the stir zone sampled transversally, while Figure 4(b) depicts the longitudinally sampled specimen. To determine grain size in Figure 4(a), a recurring application of the linear intercept method was employed at various locations. The data collected from these measurements were then utilized to compute both the mean grain size and standard deviation, as detailed in Table II. Similarly, the mean grain size of the longitudinally sampled specimen was determined using a comparable methodology. However, due to its stacked configuration, the grain size measurements were taken from different vertical locations, leading to the presentation of L1-L3 data in Table II. Figure 5 offers insight into the microstructural grain distribution in relation to Figure 4. In the transversely sampled specimen, the mean grain size measured was 11.48 µm, with a standard deviation of 3.57 µm. In contrast, the longitudinally sampled specimen exhibited varying mean grain sizes within the range of 7.32 µm to 15.09 µm. This fluctuation in grain size indicates that different regions of the joint underwent dynamic recrystallization to varying degrees. It should be noted that the L3 region, which is closer to the surface in contact with the weld bed, displayed a defect-free nature and was dominated by exceptionally refined grains. This is attributed to the influence of the bed surface, where dynamic recrystallization and plastic flow are effectively controlled [27]. Furthermore, the longitudinally sampled specimen revealed the emergence of the strengthening precipitate, known as magnesium-iron, resulting from the interaction between AA8011 and AA6082 alloys [28].

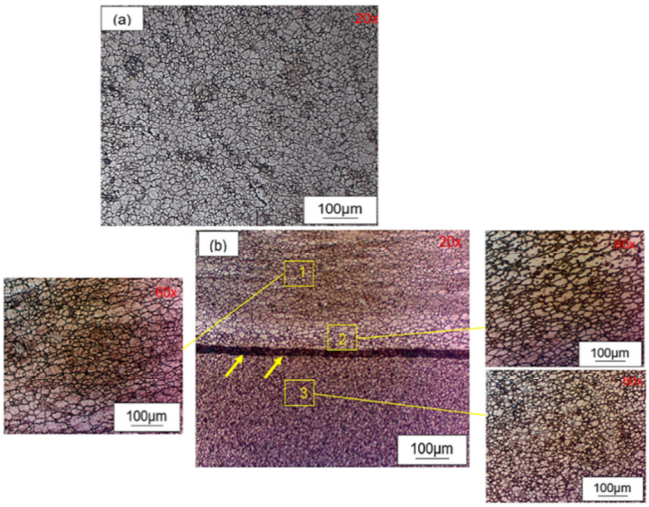

Fig. 4. (a) FSP+TIG microstructural arrangement of the stir zone sampled (a) transversally, (b) longitudinally.

TABLE II. MEAN GRAIN SIZE AND STANDARD DEVIATION.

Joint	Mean grain size (µm)	Standard deviation (µm)
Transverse	11.48	3.57
Longitudinal L1	12.48	3.84
Longitudinal L2	15.09	6.74
Longitudinal L3	7.32	2.68

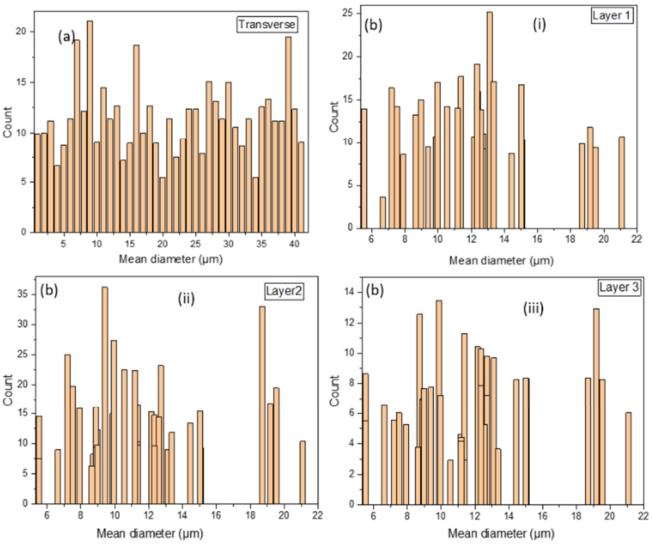

Fig. 5. Grain size distribution for (a) the transversally sampled specimen, (b) the longitudinally sampled specimen (i-iii).

B. Tensile Properties

The tensile specimens' post-tensile test results are shown in Figure 6(a), while Figure 6(b) shows the corresponding stress-strain graphs. The corresponding results are presented in Table III. The transversally sampled specimen failed at the center of the stir zone, while the longitudinally sampled specimen failed at the middle of the specimen. The transversally sampled specimen underwent a clear necking mechanism before fracture, while the longitudinally sampled specimen shows

unclear necking. The necking symbolizes that FSP did not bring enough microstructural defects healing at the center of the joint, thereby making this region the target for the failure initiation site. This failure also suggests that a nonuniform microstructural arrangement dominates the specimen. The stress-strain curves in Figure 6(b) clearly distinguish between the joint's tensile properties when subjected to transversal and longitudinal loads. The tensile strength of the specimen sampled longitudinally is higher than that of the transversally sampled specimen. The Ultimate Tensile Stress (UTS) values for the longitudinally and transversally sampled specimens are 133.83 MPa and 87.88 MPa, respectively. The tensile strain at UTS for longitudinally and transversally sampled specimens are 19.36% and 10.89%, respectively. The tensile strain values at the breakpoint for the longitudinally and transversally sampled specimens are 26.64% and 27.49%, respectively. The tensile properties of the longitudinally sampled specimen are higher than those of the transversally sampled specimen. This longitudinally sampled specimen's dominance in tensile properties is due to the fact that this specimen is dominated by refined grains observed during the microstructural analysis [29-31]. The refined grains contribute immensely to the tensile properties of the materials according to Hall-Patch relationship [32]. It is good to note that the longitudinally sampled specimens exhibit UTS that is way higher than AA8011 parent material and TIG welded joint but lower than AA6082 parent material. The UTS for transversally sampled specimens exhibits UTS that is lower than both parent materials but higher than the TIG welded joint [10, 33].

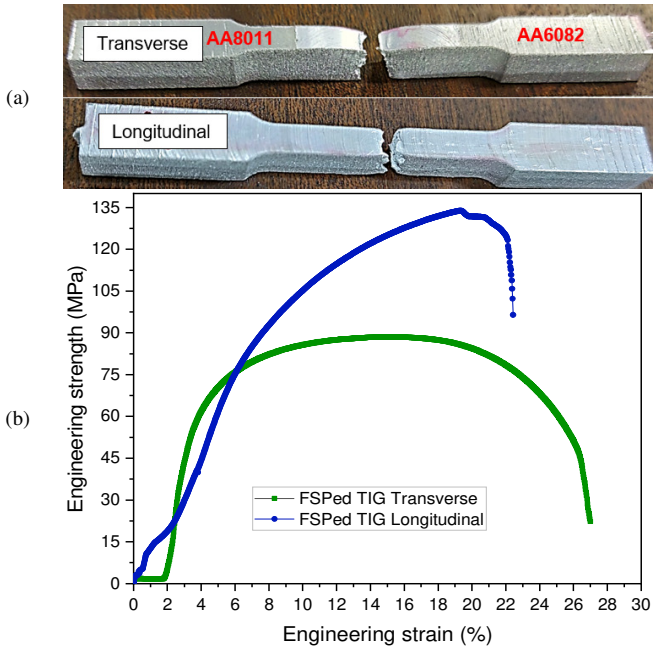

Fig. 6. (a) Fractured tensile specimens and (b) engineering stress–strain curves.

C. Fractography

Figures 7(a)-(b) show the fractography for the transversally and longitudinally sampled specimens, respectively. It should be noted that the specimens fractured at the middle of the joint (transversally sampled specimen) and the specimen (longitudinally sampled specimen). Dimples of different sizes characterize the fractured surface of both specimens, which are ductile fracture characteristics. Numerous pores and voids are detected on the fractured surface of the transversally sampled specimen. These defects result from insufficient material flow and mixing, which contribute to the weakening of the joint. Dimples of different sizes dominate the longitudinally sampled specimen, suggesting ductile failure [10, 32-34].

TABLE III. TENSILE PROPERTIES

FSPed TIG	Ultimate tensile strength (MPa)	Tensile strain at UTS (%)	Tensile strain at breakpoint (%)	Position of fracture
Transverse	87.88	10.89	27.49	SZ
Longitudinal	133.83	19.36	26.64	Center

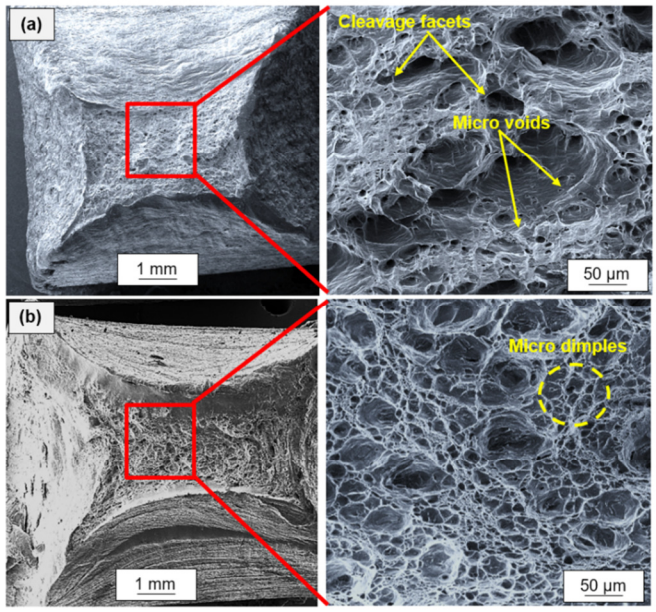

Fig. 7. Fractography for (a) transversally sampled specimen and (b) longitudinally sampled specimen.

D. Microhardness

Figure 8 depicts the microhardness profiles for transversally and longitudinally sampled specimens. The transversally sampled specimen shows a varying trend from the AA6082 base material toward the stir zone and a decreasing trend from the stir zone toward the AA8011 base material. This is a generic behavior for a joint composed of two dissimilar materials. The maximum microhardness at the stir zone for the transversally sampled specimen was 57 HV which is slightly higher than the TIG welded joint, followed by the sharp decrease toward the AA8011 side of the stir zone [10, 33, 36-38]. The sharp decrease may be caused by microstructural defects emerging from insufficient material mixing. The microhardness for the longitudinally sampled specimen shows a fluctuation across the thickness of the specimen, which is attributed to the variation in gran size observed during microstructural analysis. This is a manifestation of the joint composed of two dissimilar materials with unique mechanical

properties [39, 40]. The microhardness of the two specimens' configuration was found to be higher than that of the parent materials [33]. It was further observed that the microhardness profile involving dissimilar materials always follows an "S" shape unlike the "W" shape reported in the literature [41, 42].

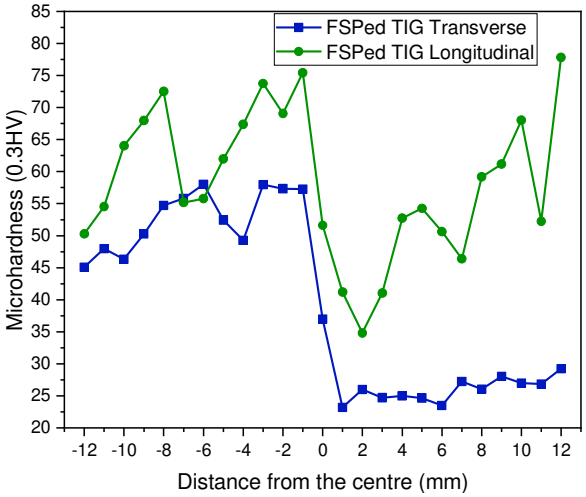

Fig. 8. Microhardness profiles of the FSPed TIG weldments.

IV. CONCLUSION

In this study, the influence of microstructural arrangement on the mechanical properties of the friction stir processed TIG-welded joints with the main focus on the sampling direction was investigated. Based on the obtained results, the following conclusions were drawn:

- The microstructural arrangement of the joint varies with sampling directions. This was manifested during the measurement of the grain, where different locations of the longitudinally sampled specimen had different grain sizes. Another feature (strengthening precipitate) was also detected through the microstructural analysis of the longitudinally sampled specimen, which was not visible on a transversally sampled specimen.
- The tensile properties of the longitudinally sampled joint are way higher than those of the transversally sampled joint. This suggests that the joint responds differently to longitudinal and transversal loads.
- The fracture mechanisms for both longitudinal and transversal directions are similar, but the transversally sampled specimen showed some defects.
- The microhardness profile for both specimens is unique, and this uniqueness is due to the microstructural difference observed during microstructural analysis.

ACKNOWLEDGMENT

The authors thank the National Research Foundation [KIC2208114986] for funding this study.

REFERENCES

[1] G. Singh, A. S. Kang, K. Singh, and J. Singh, "Experimental comparison of friction stir welding process and TIG welding process for 6082-T6 Aluminium alloy," *Materials Today: Proceedings*, vol. 4, no. 2, Part A, pp. 3590–3600, Jan. 2017, https://doi.org/10.1016/j.matpr.2017.02.251.

[2] R. Kumar *et al.*, "A comparative analysis of friction stir and tungsten inert gas dissimilar AA5082-AA7075 butt welds," *Materials Science for Energy Technologies*, vol. 5, pp. 74–80, Jan. 2022, https://doi.org/10.1016/j.mset.2021.12.002.

[3] Y. S. Sato, M. Urata, and H. Kokawa, "Parameters controlling microstructure and hardness during friction-stir welding of precipitation-hardenable aluminum alloy 6063," *Metallurgical and Materials Transactions A*, vol. 33, no. 3, pp. 625–635, Mar. 2002, https://doi.org/10.1007/s11661-002-0124-3.

[4] Y. Huang, P. Liu, H. Xiang, S. Deng, Y. Guo, and J. Li, "Mechanical properties, corrosion and microstructure distribution of a 2195-T8 AlLi alloy TIG welded joint," *Journal of Manufacturing Processes*, vol. 90, pp. 151–165, Mar. 2023, https://doi.org/10.1016/j.jmapro.2023.02.007.

[5] N. A. Liyakat and D. Veeman, "Improvement of mechanical and microstructural properties of AA 5052-H32 TIG weldment using friction stir processing approach," *Journal of Materials Research and Technology*, vol. 19, pp. 332–344, Jul. 2022, https://doi.org/10.1016/j.jmrt.2022.05.015.

[6] X. Yang *et al.*, "Microstructures and microhardness for sheets and TIG welded joints of TA15 alloy using friction stir spot processing," *Transactions of Nonferrous Metals Society of China*, vol. 28, no. 1, pp. 55–65, Jan. 2018, https://doi.org/10.1016/S1003-6326(18)64638-2.

[7] H. Mehdi and R. S. Mishra, "Effect of friction stir processing on mechanical properties and heat transfer of TIG welded joint of AA6061 and AA7075," *Defence Technology*, vol. 17, no. 3, pp. 715–727, Jun. 2021, https://doi.org/10.1016/j.dt.2020.04.014.

[8] H. Mehdi and R. S. Mishra, "Investigation of mechanical properties and heat transfer of welded joint of AA6061 and AA7075 using TIG+FSP welding approach," *Journal of Advanced Joining Processes*, vol. 1, Mar. 2020, Art. no. 100003, https://doi.org/10.1016/j.jajp.2020.100003.

[9] H. H. Jadav, V. Badheka, D. K. Sharma, and G. Upadhyay, "A review on effect of friction stir processing on the welded joints," *Materials Today: Proceedings*, vol. 43, pp. 84–92, Jan. 2021, https://doi.org/10.1016/j.matpr.2020.11.215.

[10] S. Mabuwa, V. Msomi, O. Muribwathoho, and S. Saasebeng Motshwanedi, "The microstructure and mechanical properties of the friction stir processed TIG-welded aerospace dissimilar aluminium alloys," *Materials Today: Proceedings*, vol. 46, pp. 658–664, Jan. 2021, https://doi.org/10.1016/j.matpr.2020.11.588.

[11] A. Thakur, V. Sharma, N. Minhas, S. Manda, and V. S. Sharma, "Microstructure and mechanical properties of dissimilar friction stir welded joints of laser powder bed fusion processed AlSi10Mg and conventional hot rolled 6061-T6 thin sheets," *Optics & Laser Technology*, vol. 163, Aug. 2023, Art. no. 109382, https://doi.org/10.1016/j.optlastec.2023.109382.

[12] M. Kumar, A. Das, and R. Ballav, "Influence of the Zn interlayer on the mechanical strength, corrosion and microstructural behavior of friction stir-welded 6061-T6 aluminium alloy and AZ61 magnesium alloy dissimilar joints," *Materials Today Communications*, vol. 35, Jun. 2023, Art. no. 105509, https://doi.org/10.1016/j.mtcomm.2023.105509.

[13] K. M. Mehta and V. J. Badheka, "Wear behavior of Al-6061-B4C surface composites fabricated by Friction Stir Processing using Slot and Hole method of reinforcement application," *Wear*, vol. 522, Jun. 2023, Art. no. 204719, https://doi.org/10.1016/j.wear.2023.204719.

[14] S. Ghouse Mohiddin and S. Venkatesh, "Influence of reinforcement on weld bead characteristics of friction stir processed Al5083/NFA composite," *Materials Today: Proceedings*, vol. 56, pp. 1614–1617, Jan. 2022, https://doi.org/10.1016/j.matpr.2022.02.651.

[15] I. Dinaharan, S. Zhang, G. Chen, and Q. Shi, "Assessment of Ti-6Al-4V particles as a reinforcement for AZ31 magnesium alloy-based composites to boost ductility incorporated through friction stir processing," *Journal of Magnesium and Alloys*, vol. 10, no. 4, pp. 979–992, Apr. 2022, https://doi.org/10.1016/j.jma.2020.09.026.

[16] S. Choudhary and V. Gaur, "Enhanced fatigue properties of AA5086 friction stir weld joints by Cu-reinforcement," *Materials Science and Engineering: A*, vol. 869, Mar. 2023, Art. no. 144778, https://doi.org/10.1016/j.msea.2023.144778.

[17] J. S. Jesus, J. M. Costa, A. Loureiro, and J. M. Ferreira, "Fatigue strength improvement of GMAW T-welds in AA 5083 by friction-stir processing," *International Journal of Fatigue*, vol. 97, pp. 124–134, Apr. 2017, https://doi.org/10.1016/j.ijfatigue.2016.12.034.

[18] H. Mehdi and R. S. Mishra, "Study of the influence of friction stir processing on tungsten inert gas welding of different aluminum alloy," *SN Applied Sciences*, vol. 1, no. 7, Jun. 2019, Art. no. 712, https://doi.org/10.1007/s42452-019-0712-0.

[19] H. Mehdi and R. S. Mishra, "An experimental analysis and optimization of process parameters of AA6061 and AA7075 welded joint by TIG+FSP welding using RSM," *Advances in Materials and Processing Technologies*, vol. 8, no. 1, pp. 598–620, Jan. 2022, https://doi.org/10.1080/2374068X.2020.1829952.

[20] S. Mabuwa and V. Msomi, "The effect of friction stir processing on the friction stir welded AA1050-H14 and AA6082-T6 joints," *Materials Today: Proceedings*, vol. 26, pp. 193–199, Jan. 2020, https://doi.org/10.1016/j.matpr.2019.10.039.

[21] H. Mehdi and R. S. Mishra, "Effect of Friction Stir Processing on Mechanical Properties and Wear Resistance of Tungsten Inert Gas Welded Joint of Dissimilar Aluminum Alloys," *Journal of Materials Engineering and Performance*, vol. 30, no. 3, pp. 1926–1937, Mar. 2021, https://doi.org/10.1007/s11665-021-05549-y.

[22] H. Mehdi and R. S. Mishra, "Effect of Friction Stir Processing on Microstructure and Mechanical Properties of TIG Welded Joint of AA6061 and AA7075," *Metallography, Microstructure, and Analysis*, vol. 9, no. 3, pp. 403–418, Jun. 2020, https://doi.org/10.1007/s13632-020-00640-7.

[23] H. Mehdi and R. Mishra, "Microstructure and mechanical characterization of tungsten inert gas-welded joint of AA6061 and AA7075 by friction stir processing," *Proceedings of the Institution of Mechanical Engineers, Part L: Journal of Materials: Design and Applications*, vol. 235, no. 11, pp. 2531–2546, Dec. 2021, https://doi.org/10.1177/14644207211007882.

[24] A. N. Salah, S. Mabuwa, H. Mehdi, V. Msomi, M. Kaddami, and P. Mohapatra, "Effect of Multipass FSP on Si-rich TIG Welded Joint of Dissimilar Aluminum Alloys AA8011-H14 and AA5083-H321: EBSD and Microstructural Evolutions," *Silicon*, vol. 14, no. 15, pp. 9925–9941, Oct. 2022, https://doi.org/10.1007/s12633-022-01717-4.

[25] A. W. Hashmi, H. Mehdi, S. Mabuwa, V. Msomi, and P. Mohapatra, "Influence of FSP Parameters on Wear and Microstructural Characterization of Dissimilar TIG Welded Joints with Si-rich Filler Metal," *Silicon*, vol. 14, no. 17, pp. 11131–11145, Nov. 2022, https://doi.org/10.1007/s12633-022-01848-8.

[26] V. Msomi and S. Mabuwa, "Analysis of material positioning towards microstructure of the friction stir processed AA1050/AA6082 dissimilar joint," *Advances in Industrial and Manufacturing Engineering*, vol. 1, Nov. 2020, Art. no. 100002, https://doi.org/10.1016/j.aime.2020.100002.

[27] H. Yamamoto, Y. Danno, K. Ito, Y. Mikami, and H. Fujii, "Weld toe modification using spherical-tip WC tool FSP in fatigue strength improvement of high-strength low-alloy steel joints," *Materials & Design*, vol. 160, pp. 1019–1028, Dec. 2018, https://doi.org/10.1016/j.matdes.2018.10.036.

[28] B. Mvola, P. Kah, and J. Martikainen, "Welding of dissimilar non-ferrous metals by GMAW processes," *International Journal of Mechanical and Materials Engineering*, vol. 9, no. 1, Oct. 2014, Art. no. 21, https://doi.org/10.1186/s40712-014-0021-8.

[29] P. He, X. Bai, and H. Zhang, "Microstructure refinement and mechanical properties enhancement of wire and arc additively manufactured 6061 aluminum alloy using friction stir processing post-treatment," *Materials Letters*, vol. 330, Jan. 2023, Art. no. 133365, https://doi.org/10.1016/j.matlet.2022.133365.

[30] J. Wei, C. He, Y. Zhao, M. Qie, G. Qin, and L. Zuo, "Evolution of microstructure and properties in 2219 aluminum alloy produced by wire arc additive manufacturing assisted by interlayer friction stir processing," *Materials Science and Engineering: A*, vol. 868, Mar. 2023, Art. no. 144794, https://doi.org/10.1016/j.msea.2023.144794.

[31] J. Wei *et al.*, "Microstructure refinement and mechanical properties enhancement of wire-arc additive manufactured 2219 aluminum alloy assisted by interlayer friction stir processing," *Vacuum*, vol. 203, Sep. 2022, Art. no. 111264, https://doi.org/10.1016/j.vacuum.2022.111264.

[32] Y. Li, A. J. Bushby, and D. J. Dunstan, "The Hall–Petch effect as a manifestation of the general size effect," *Proceedings of the Royal Society A: Mathematical, Physical and Engineering Sciences*, vol. 472, no. 2190, Jun. 2016, Art. no. 20150890, https://doi.org/10.1098/rspa.2015.0890.

[33] S. Mabuwa and V. Msomi, "Fatigue behaviour of the multi-pass friction stir processed AA8011-H14 and AA6082-T651 dissimilar joints," *Engineering Failure Analysis*, vol. 118, Dec. 2020, Art. no. 104876, https://doi.org/10.1016/j.engfailanal.2020.104876.

[34] M. Verma and P. Saha, "Effect of micro-grooves featured tool and their depths on dissimilar micro-friction stir welding (μFSW) of aluminum alloys: A study of process responses and weld characteristics," *Materials Characterization*, vol. 196, Feb. 2023, Art. no. 112614, https://doi.org/10.1016/j.matchar.2022.112614.

[35] T. Madani, M. Boukraa, M. Aissani, T. Chekifi, A. Ziadi, and M. Zirari, "Experimental investigation and numerical analysis using Taguchi and ANOVA methods for underwater friction stir welding of aluminium alloy 2017 process improvement," *International Journal of Pressure Vessels and Piping*, vol. 201, Feb. 2023, Art. no. 104879, https://doi.org/10.1016/j.ijpvp.2022.104879.

[36] C. He *et al.*, "Improvement of microstructure and fatigue performance of wire-arc additive manufactured 4043 aluminum alloy assisted by interlayer friction stir processing," *Journal of Materials Science & Technology*, vol. 133, pp. 183–194, Jan. 2023, https://doi.org/10.1016/j.jmst.2022.07.001.

[37] B. V. G. de Viveiros, R. M. P. da Silva, U. Donatus, and I. Costa, "Welding and galvanic coupling effects on the electrochemical activity of dissimilar AA2050 and AA7050 aluminum alloys welded by Friction Stir Welding (FSW)," *Electrochimica Acta*, vol. 449, May 2023, Art. no. 142196, https://doi.org/10.1016/j.electacta.2023.142196.

[38] S. Raj and P. Biswas, "Effect of induction preheating on microstructure and mechanical properties of friction stir welded dissimilar material joints of Inconel 718 and SS316L," *CIRP Journal of Manufacturing Science and Technology*, vol. 41, pp. 160–179, Apr. 2023, https://doi.org/10.1016/j.cirpj.2022.12.014.

[39] N. Dimov *et al.*, "Strain and damage analysis using high resolution digital image correlation in the stir zone of an AA6061-AA7075 dissimilar friction stir weld," *Materials Today Communications*, vol. 34, Mar. 2023, Art. no. 105359, https://doi.org/10.1016/j.mtcomm.2023.105359.

[40] A. W. El-Morsy, M. Ghanem, and H. Bahaitham, "Effect of Friction Stir Welding Parameters on the Microstructure and Mechanical Properties of AA2024-T4 Aluminum Alloy," *Engineering, Technology & Applied Science Research*, vol. 8, no. 1, pp. 2493–2498, Feb. 2018, https://doi.org/10.48084/etasr.1704.

[41] J. A. Al-jarrah, A. Ibrahim, and S. Sawlaha, "Effect of Applied Pressure on the Mechanical Properties of 6061 Aluminum Alloy Welded Joints Prepared by Friction Stir Welding," *Engineering, Technology & Applied Science Research*, vol. 7, no. 3, pp. 1619–1622, Jun. 2017, https://doi.org/10.48084/etasr.1124.

[42] M. Elitas and B. Demir, "The Effects of the Welding Parameters on Tensile Properties of RSW Junctions of DP1000 Sheet Steel," *Engineering, Technology & Applied Science Research*, vol. 8, no. 4, pp. 3116–3120, Aug. 2018, https://doi.org/10.48084/etasr.2115.